Langmuir

Article

pubs.acs.org/Langmuir

Potential Toxicity of Up-Converting Nanoparticles Encapsulated with a Bilayer Formed by Ligand Attraction

Gautom K. Das,[†] Daniel T. Stark,[†] and Ian M. Kennedy*

Department of Mechanical and Aerospace Engineering, University of California, One Shields Avenue, Davis, California 95616, United States

Supporting Information

ABSTRACT: The cellular toxicity of nanoparticles that were capped with a bilayered ligand was studied using an up-converting (UC) phosphor material as a representative nanoparticle (NP). The results indicate that although UC NPs are known to be nontoxic, the toxicity of the NPs depends strongly on ligand coordination conditions, in addition to the other commonly known parameters such as size, structure, surface charge etc. Oleate-capped hydrophobic $NaYF_4$:Yb,Er NPs were surface modified to yield three extreme conditions: bare particles that were stripped of the oleate ligands; particles with covalently bound poly(ethylene glycol) (PEG) ligands; and particles with an bilayer of PEG-oleate ligands using the oleate surface group that was remained after synthesis. It was found that the bare particles and the covalent PEG NPs induced little toxicity. However, particles that were rendered biocompatible by forming a bilayer with an amphiphilic ligand (i.e., PEG-oleate) resulted in significant cell toxicity. These findings strongly suggest that the PEG-oleate group dissociated from the bilayered oleate-capped NPs, resulting in significant toxicity by exposing the hydrophobic oleate-capped NPs to the cell. Based on results with bare particles, the $NaLnF_4$:Yb,Er (Ln = Y, Gd) up-converting phosphors are essentially less-toxic. Capping and functionalizing these particles with ligand intercalation may, however, not be a suitable method for rendering the NPs suitable for bioapplication as the ligand can potentially dissociate upon cellular interaction, leading to significant toxicity.

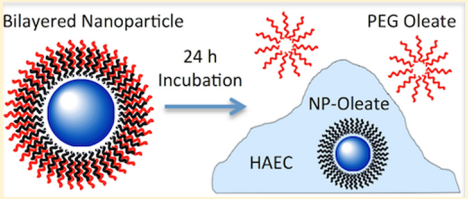

INTRODUCTION

Most synthetic routes to high-quality nanoparticles (NPs), with respect to uniformity, size control, and crystallinity, generally make use of organic solutions and predominantly employ long-chain hydrocarbons that contain a coordinating headgroup such as oleic acid (OA) as the ligand to sterically stabilize NPs in nonpolar, hydrophobic solvents.[1] However, biological applications require NPs to be fully dispersible in hydrophilic or aqueous media without degradation of their properties. Therefore, organically-synthesized hydrophobic NPs need to go through a surface modification process before use in bioapplications.[2−13]

The first general approach to such surface modification entails replacement of the original ligands by a specially designed hydrophilic species through coordinate bonding in a process known as ligand exchange.[12,14,15] While this approach is very practical and widely used, one major limitation of this method is that most of the ligand-exchange reactions employ stronger surface binding molecules that replace the original ligand, often yielding an irreversible ligand exchange, thus making it difficult for further functionalization of the NPs. Another popular approach, known as ligand attraction, uses hydrophobic van der Waals interactions, through which the hydrophobic tail of an amphiphilic ligand interacts with, but does not replace, the hydrophobic ligand on nanocrystals and leads to the complete encapsulation of the NP core through a bilayer formation; the hydrophilic part renders the NPs fully dispersible in aqueous media.[5,7,12,16−18] In the ligand attraction method, the original ligand layers do not get replaced—the particle dispersity of the newly functionalized NPs is nearly as good as the original NPs solution with almost no aggregation.[12,16,17]

The nature of the surface ligands on NPs is an important consideration in determining their stability as well as toxic effects in biological systems. Depending on the nanoparticle type and the solvent in which the particles are dispersed, the choice of appropriate ligand may not only provide the stability of the NPs but also prevent any aggregation in solution. Therefore, the ligand molecules have to be bound to the NPs surface by some kind of attractive interaction, for example, by chemisorption, electrostatic attraction, or hydrophobic interaction.[12] Though different types of ligands and attachment strategies have been developed for efficient use of NPs, ligands are highly sensitive to conditions such as solution pH, ionic concentration, and the nature of the interactions, which can lead to dissociation from the NPs.[5,12,19,20]

We have chosen to study an up-converting phosphor NP ($NaYF_4$:Yb,Er) as representative of a subset of the class of particles with high potential for future biological applications.[21−25] During up-conversion, long wavelength, low energy photons are absorbed, leading to the emission of shorter wavelength, higher energy photons. These NPs offer unique

Received: April 24, 2014
Revised: June 8, 2014
Published: June 27, 2014

   dx.doi.org/10.1021/la501595f | Langmuir 2014, 30, 8167−8176

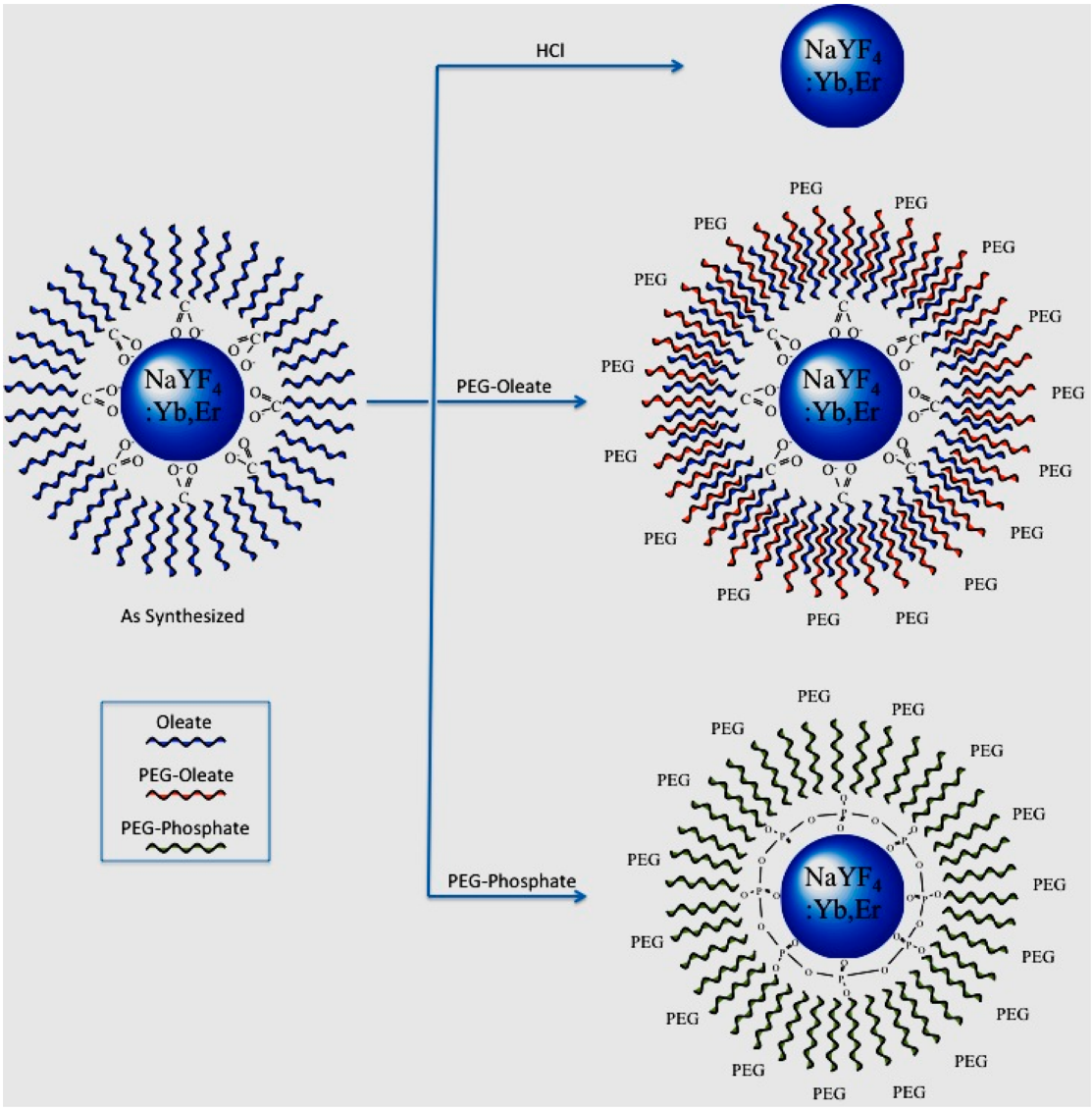

Figure 1. Schematic of surface modification of the oleate-capped $NAYF_4$:Yb,Er NPs as (i) ligand-free (top), (ii) PEG-oleate bilayered (middle), and (iii) covalently bound PEG NPs (bottom).

optical properties for biolabeling, including narrow emission band-widths, large anti-Stokes shifts, long luminescence lifetimes, and excellent photostability, making them more attractive for use as biomarkers than conventional organic dyes or quantum dots.[26−30] Similarly to other controlled synthesis methods of NPs, the up-converting phosphors are commonly synthesized in organic media followed by postsynthesis modification of their surfaces, especially for bioapplications. Importantly, this class of NPs is known to be less toxic than its counterparts such as quantum dots.[9−11,31,32]

Although the cytotoxicity of NPs generally depends on a number of critical parameters such as particle size, shape, surface charge, hydrophobicity and the nature of the surface ligands, up-converting NPs have only been tested for a limited range of functionalization chemistries.[8−11] Therefore, there is a clear need to test this class of materials at different conditions, especially under different surface-ligand binding conditions, which are critical for maintaining biocompatibility.

To assess the fate of the NPs under physiological conditions, we have engineered NPs with three types of surface conditions: (i) particles with no ligands (i.e., bare surface NPs); (ii) particle with an additional biocompatible ligand layer attached by hydrophobic ligand attraction; and (iii) particles with a biocompatible ligand that is covalently bound to the surface. Poly(ethylene glycol) (PEG) was chosen as the hydrophilic ligand for its extreme good biocompatibility, which renders stability to nanoparticles and prevent undesired protein adhesion. A hydrophobic oleate-coupled PEG was chosen as the amphiphilic ligand for the bilayer formation as oleic acid is one of the extensively used hydrophobic ligand used for nanoparticle synthesis. A number of PEG-coupled amphiphilic ligands have been reported in the literature for hydrophobic ligand attraction mediated phase transfer such as octylamine−poly(acrylic acid)−poly(ethylene glycol) (OA−PAA−PEG),[33] poly(ethylene glycol)-*block*-poly(carprolactone) (PEG-*b*-PCL),[34] poly((ethylene glycol)-*block*-lactic acid) (PEG-*b*-PLA),[34] and poly(ethylene glycol) monooleate (PEG-OA).[18,35] We focused on PEG-monooleate for this study as it forms an oleate−oleate hydrophobic bilayer with the synthesized oleate-capped up-converting NPs and minimally affects the original surface conditions of the NPs. For covalent binding, PEG-phosphate was used as the ligand for its

dx.doi.org/10.1021/la501595f | *Langmuir* 2014, 30, 8167−8176

widespread use in similar usage. The interaction of the cells with these types of NPs can provide general insight into the potential for toxic effects due to the different surface conditions for any organically synthesized nanomaterial.

MATERIALS AND METHODS

To understand the interaction, the as-synthesized $NaYF_4$:Yb,Er (i.e., oleate-capped $NaYF_4$:Yb,Er) NPs were specifically modified as follows: (i) $NaYF_4$:Yb,Er with no ligands; (ii) $NaYF_4$:Yb,Er NPs coated with a PEG-oleate bilayer; and (iii) covalently bound PEG-$NaYF_4$:Yb,Er NPs (Figure 1). Cytotoxicity was assessed with an MTT enzymatic activity assay that was confirmed by a calcein−propidium iodide live/dead cell viability assay.

Synthesis of Nanoparticles. *Chemicals.* All chemicals were used as received without further purifications. Yttrium chloride hexahydrate (> 99.9%), erbium chloride hexahydrate (> 99.995%), ytterbium chloride hexahydrate (> 99.9%), oleic acid (tech., 90%), 1-octadecene (tech., 90%), ammonium fluoride (> 99.99%), sodium hydroxide (pellets, reagent grade >98%), poly(ethylene glycol) ($M_n \sim 2000$), PEG monooleate ($M_n \sim 860$) were purchased from Sigma-Aldrich. Cyclohexane and hydrochloric acid were purchased from EMD, hexane (ACS, ≥ 98.5%), methanol (ACS, 99%), and ethanol were purchased from Fisher Scientific, and chloroform (ACS, 99.8%) was purchased from Alfa Aesar.

Synthesis of NaYF4:Yb,Er NPs. Oleate-capped $NaYF_4$:Yb,Er NPs were synthesized using a high-temperature synthesis method developed by Li and Zhang.[36] Typically, 0.8 mmol of YCl3·6H2O, 0.18 mmol of YbCl3·6H2O, and 0.02 mmol of ErCl3·6H2O were dissolved in a mixture of 6 mL oleic acid and 15 mL 1-octadecene and heated to 120 °C under vacuum for 2 h. The mixture was cooled to room temperature and a solution of 2.5 mmol NaOH and 2.5 mmol NH4F dissolved in 10 mL methanol was added. The resulting mixture was further stirred for 30 min at room temperature and then slowly heated to 70 °C to remove methanol. Once methanol was removed, the resulting solution was heated to 300 °C under an argon atmosphere and kept for 1 h. Subsequently, the solution was cooled down to room temperature and precipitated with ethanol. The NPs were washed several times with ethanol and collected by centrifugation. The washed NPs were dispersed in 5 mL chloroform for further surface modification and characterization.

Transfer into Water as Ligand-Free (Oleate-Free) $NaYF_4$:Yb,Er NPs. The synthesis approach is based on removing the oleate ligands from the surface of as-synthesized NPs using an acid treatment process as developed by Bogdan et al.[37] Typically, the as-synthesized oleate-capped NPs (50 mg) were dispersed in 10 mL cyclohexane, then 20 mL of 0.1 M HCl (pH = 3) was introduced. After vigorous stirring for 3 h, the NPs were transferred from the upper cyclohexane to the water below. During the reaction the carboxylate groups of the oleate ligands were protonated to yield oleic acid. After separating the aqueous layer, oleic acid was extracted using diethyl ether three times. The NPs in the water dispersible fraction were collected by centrifugation and were rinsed by acetone. The NPs were then dispersed in water and collected by ultracentrifugation at 100 000*g* for 1 h. The pellets were redispersed in 10 mL milli-Q water (18 MΩ) for further use.

Transfer into Water as PEG-Oleate Bilayered $NaYF_4$:Yb,Er NPs. The phase transfer protocol was adapted from the method developed by Colvin et al.[5] Typically, 1 mL of NPs (0.2 mmol) dispersion in chloroform (i.e., stock solution of the oleate-capped NPs) was added to 500 mg PEG-Monooleate dissolved in 9 mL chloroform. The solution was stirred overnight at room temperature. Then, chloroform was removed slowly under vacuum at room temperature, leaving a waxy layer at the bottom of the flask. About 15 mL of milli-Q water (18 MΩ) was added to the waxy liquid and dispersed very well by sonication (2510 Branson Ultrasonic Cleaner) for 30 min. The murky solution slowly became transparent with sonication. The flask was put under vacuum and the remaining chloroform was removed slowly at room temperature. The NPs were collected using a microcentrifuge (accuSpin Micro, Fisher Scientific) at a speed of 13 000 rpm for 10 min. The collected pellet was redispersed in milli-Q water to a concentration of 7.8 mg/mL for cell study. NPs were further diluted in DPBS to 2000 μg/mL. This stock solution was used for all subsequent experiments. Nanoparticle stock solutions were ultrasonicated for 5 min immediately prior to final dilution in culture medium for cell exposure.

Transfer into water as covalently bound PEG-$NaYF_4$:Yb,Er NPs. Covalently bound PEG- $NaYF_4$:Yb,Er NPs were synthesized using a modified protocol developed by Boyer et al.[38] Approximately, 50 mg of ligand free nanoparticles dispersed in 2 mL of absolute ethanol were taken into a 20 mL glass vial and 300 mg of PEG (750)-phosphate ligand was added to it. The vial was capped tightly and the resulting solution was stirred overnight at 60 °C. It was then cooled to room temperature, and NPs were collected via centrifugation at 10000 rpm. The resulted pellet was redispersed in milli-Q water for further experimentation.

Characterization of the Nanoparticles. Transmission electron microscopy (TEM) images were recorded using a Philips CM-12 TEM equipped with a CCD camera operating at 120 kV. The samples were prepared by drop-casting the NP dispersions on a formvar-coated 400-mesh copper TEM grid and air-dried. Powder X-ray diffraction (XRD) pattern of the NPs were collected using a Scintag powder X-ray diffractometer (XRD) with Cu Kα radiation (λ= 1.54056 Å, operated at 45 kV and 40 mA) with 4 mm divergence slit, 1 mm scattering slit, and 0.2 mm receiving slit. The scanning step size was 0.015° in 2θ with a counting time of 1 s per step.

The hydrodynamic size distribution and state of agglomeration/dispersion of the NPs was analyzed by dynamic light scattering (DLS) technique using a Brookhaven ZetaPlus instrument (Brookhaven Instrument Inc. Holtsville, NY). The particle size distributions were calculated by the 90Plus software (Brookhaven Instruments). The Zeta Potential (ZP) of the NP samples was determined using the same ZetaPlus instrument (Brookhaven Instruments Corp.).

The NPs were excited by a continuous wave laser (Lasermate) operating at 980 nm. A Princeton Instruments PI-MAX camera fitted with a charge-coupled device sensor and an Acton Spectrapro 300i series spectrometer were used to collect the up-converted emission from quartz cuvettes. The laser was operated with a power density of 67 W/cm^{-2}.

Fourier transformation infrared (FTIR) spectra were collected using a Thermo Scientific Nicolet IR100 Spectrometer (Fisher Scientific) to quantitatively compare FTIR spectra before and after ligand exchange, and at different surface conditions. The absorbance was normalized and the spectra were baseline-corrected. Thermogravimetric analysis (TGA) was conducted using a Setsys Evolution 1600 TG/DSC (Setaram Instrumentation, Caluire, France) at a heating rate

dx.doi.org/10.1021/la501595f | Langmuir 2014, 30, 8167−8176

of 10 °C/min in air to determine the percent of organic content on the NPs.

Cell Culture. Primary Human Aortic Endothelial Cells (HAECs) were procured from Lifeline Cell Technologies (FC-0014) and cultured in Vasculife VEGF cell culture medium containing 2% FBS, 10 mM L-Glutamine, 0.75 U/ml Heparin Sulfate, 1.0 μg/mL Hydrocortisone Hemisuccinate, 50 μg/mL Ascorbic Acid, 15 ng/mL rh IGF-1, 5 ng/mL rh FGF Basic, and 5 ng/mL rh EGF at 37 °C in a humidified 5% CO_2 incubator. Cells were proliferated to 95% confluency for all experiments and were used up to passage 6. For confocal imaging, cells were cultured in glass bottom culture dishes (matTek Part Number P50G-1.5-30-F) that were treated with 5 ng/mL TI Rat tail collagen (BD Biosciences Part Number 354236) in 0.01 mM Ascorbic Acid solution for 30 min prior to cell plating.

Cells Incubation with NPs and Viability Assessment via MTT Assay. An MTT assay (Life Technologies V13154) was used to determine how the NPs affected cellular metabolic activity. Per kit instructions, cells were plated at 5000−10 000 cells per well and allowed 48 to 72 h to reach confluency, at which point NP incubation experiments were begun. After NP incubation, cells were rinsed three times in PBS to remove any loose particles before adding 100 μL of fresh media; 10 ul of 12 mM MTT in PBS was then added to each well and incubated at 37 °C for 4 h. One hundred microliters of SDS-HCL solution was added to each well and incubated for an additional 4−18 h. Samples were then mixed, and absorbance was read at 570 nm in a Molecular Devices SpectraMax M2 plate reader (Sunnyvale, CA). $NaYF_4$:Yb,Er was tested in the as-synthesized PEGylated state as well as one stripped of all surface ligands. Concentrations ranged from 5 to 75 μg/mL with 200 μL of solution per well in a 96 well culture plate. Two NP incubation times were tested, 4 and 24 h. Experiments were run in triplicate using a standard, clear, flat bottomed 96 well culture plate (Corning part number 3596).

Calcein and Propidium Iodide Viability Assay. Calcein and propidium iodide assays (Invitrogen Part # C3100MP and P3566, respectively) were used to determine cellular viability. Calcein AM is a nonfluorescent membrane permeant dye that is hydrolyzed by intracellular acetoxylmethyl ester to a fluorescent calcein conjugate which then accumulates inside the cell and can be used to indicate membrane integrity and cellular viability. Propidium iodide is a membrane impermeant nucleic acid stain that binds the DNA of dead cells and is excluded from viable cells. Passage 5 (P5) cells were plated on 50 mm glass bottom culture dishes (MatTek Part # P50G-1.5-39-F) and were grown to 95% confluency. PEGylated and ligand-free $NaYF_4$:Yb,Er NPs were then incubated for 24 h at 5 μg/mL and 75 μg/mL concentrations. The NP solution was then gently aspirated out and replaced with 3 μM calcein in DPBS and incubated for 15 min. Propidium iodide nucleic acid stain was added to a final concentration of 4 μM for the last 5 min of incubation prior to imaging.

The culture dishes were placed on an inverted Olympus IX81 Confocal Microscope and imaged using Fluoview 1000. Calcein was excited using a 488 nm Argon Ion laser and emission collected using the FITC filter set. PI was excited with a 524.5 nm Argon Ion laser and emission collected using the TRITC filter set.

Confocal Imaging for Visualization of Nanoparticle Uptake by Cells. An Olympus IX81 confocal microscope fitted with an Optoenergy 975 nm 330 mW laser driven by an Arroyo Instruments 6310 Combosource was used to obtain images of up-converting nanophosphors. Calcein fluorescence via a 488 nm Argon ion laser source was used with a FITC filter set in order to find the focus for NIR imaging. For up-converting phosphor imaging, an in-line RDM690 short pass dichroic mirror (DM) was used to filter out reflected NIR wavelengths and a long-pass 570 nm DM was used to further separate the two emission peaks of the up-converting NPs. Images were taken at 150 mW source power using a LUCPLFLN 40X objective (NA 0.6). The calcein images were later superimposed onto the fluorescent NP images using ImageJ.

Conditioned and Denatured Media Incubation with NPs. Healthy P5 or P6 HAECs were incubated at 37 °C in a 5% CO_2 humidified incubator in fresh media for a period of 24 h. The supernatant was collected via gentle aspiration for further experimentation. The supernatant was further divided into 1 mL microcentrifuge tubes, half of which were denatured at 100 °C for 4 h. PEG-oleate bilayered and ligand-free NPs were added to final concentrations of 5 μg/mL and 75 μg/mL to both the supernatant and denatured supernatant. All microcentrifuge tubes were incubated for 24 h. A nonconditioned media control was also run for each NP at a concentration of 75 μg/mL.

RESULTS AND DISCUSSION

Characterization of the NPs. The size of the as-synthesized oleate-capped NPs was 25.3 ± 3.5 nm, determined by transmission electron microscopy (TEM) (Figure 2a). The

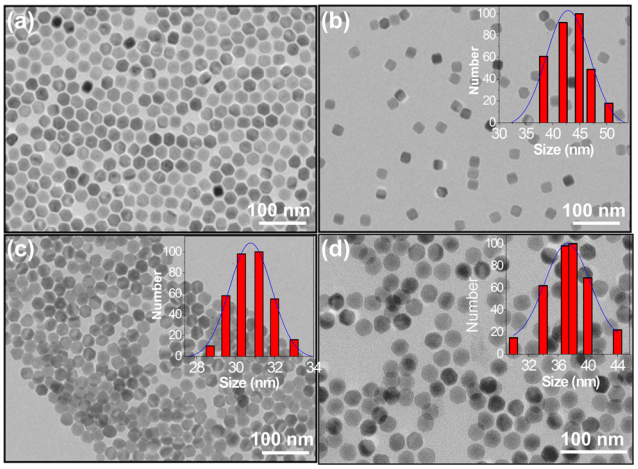

Figure 2. TEM images of (a) as-synthesized oleate-capped $NaYF_4$:Yb,Er NPs drop-cast from chloroform dispersion; phase transferred in water via (b) PEG-oleate bilayer formation; (c) ligand free (bare NPs), and (d) covalently attached PEG-NPs. Insets of the particles show the hydrodynamic size distribution obtained from DLS measurement.

PEG-oleate bilayer capped NPs, the oleate-free NPs, and the covalent coated PEG NPs exhibited similar uniformity and dispersity as can be seen in the TEM images of Figure 2 and digital photographs of NP dispersion in Figure S1. Oleic acid was the capping ligand in the organic synthesis. It is insoluble in water; however, in its bilayer form with the PEG-oleate ligands (Figure 1), the NPs contain a polar interface that yields good dispersity and stability in aqueous solution. The ligand-free (i.e., bare surface) and covalently conjugated PEG-NPs also provided a very stable dispersion in aqueous solution.

Dynamic light scattering data of the nanoparticles showed an increase in overall hydrodynamic size of the NPs compared to

dx.doi.org/10.1021/la501595f | Langmuir 2014, 30, 8167−8176

the size measured by TEM. PEG-oleate bilayer-coated NPs showed the largest hydrodynamic size (44.9 ± 6.0 nm) compared to the bare surface NPs (31.2± 2.1 nm) and covalent PEG-NPs (37.6 ± 3.2 nm) as expected (inset of Figure 2). PEG-functionalization induced a negative charge (−19 ± 1 mV) on the NPs. Stripping off the ligands (i.e., reducing them to bare NPs) transformed them to positively charged NPs (30 ± 1.7 mV) under the reaction condition (i.e., at pH ∼ 4.0). However, for the NPs dispersion at pH ∼7.0 (used for cell study) the zeta potential changes to −23± 3.7 mV. The change is zeta potential with different surface condition is shown in Figure S2. At acidic pH of reaction condition the zeta potential is positive (30 ± 1.7 mV) suggesting that in acidic conditions the oleates are protonated and detach from the NPs as oleic acid (OAH), leaving a positively charged Ln-NP. However, at pH ∼7.0 the zeta potential is negative (- 23± 3.7 mV), which suggests a deprotonated $[LnO^-]\cdots H_3O^+$ and thus a negative surface charge. The results are in good agreement with the study by Bogdan et al.[37]

FTIR spectra were taken to qualitatively determine the surface functional groups of the NPs. The spectra (Figure S3) confirmed the presence of different functional groups at every functionalization step. All the peak assignments are described and summarized in Table S1. In addition to surface characterization, powder XRD patterns of the synthesized NPs were obtained; the results are presented in Figure S4. XRD confirms the hexagonal phase of $NaYF_4$ (JCPDS # 16-0334).

Figure 3 shows a comparison of the up-conversion emission spectra of the $NaYF_4$:Yb,Er NPs with different surface

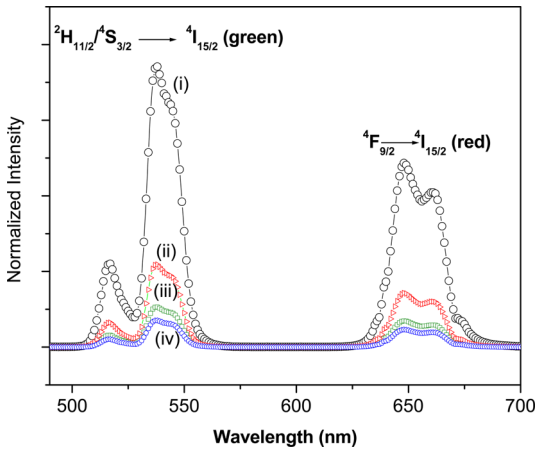

Figure 3. (a) Comparison of up-conversion luminescence spectra of $NaYF_4$:Yb,Er with different surface conditions at 980 nm excitation: (i) oleate-capped NPs in chloroform, (ii) PEG-oleate bilayered NPs in MQ water, (iii) bare surface (oleate free) NPs in MQ water, and (iv) covalently bound PEG in MQ water. All spectra were taken at 3 mg/mL concentration.

modifications, all excited at 980 nm. The spectra exhibit distinct Er^{3+} emission bands centered at 540 (green) and 650 nm (red), corresponding to $^2H_{11/2}/^4S_{3/2} \rightarrow {}^4I^{15/2}$ and $^4F_{9/2} \rightarrow {}^4I^{15/2}$ transitions of Er^{3+}, respectively. We note that the up-conversion luminescence of the surface modified NPs was decreased by a few fold in every case. PEG-oleate bilayered NPs exhibited higher luminescence compared to the other two functionalization methods. On the basis of the integrated area of the luminescence spectra, it was found that the PEG-oleate biyaler coated NPs, bare surface NPs, and the covalent-PEG NPs yielded luminescence that was reduced by 3.4, 7, and 10.5 times compared to the oleate-capped NPs in chloroform. The quenching of up-conversion luminescence has been extensively reported in the literature; it is mainly attributed to the large vibrational modes of the water molecules (∼3600 cm^{-1}) and an increase in surface defects due to the ligand modification processes.[18,37,38] However, the luminescence of the phase-transferred NPs was sufficient to be detected in a confocal microscope.

Cell-Nanoparticle Interaction. To examine the effect of ligand coordination on the cellular response, we first incubated HAEC cells with the NPs containing no ligands and with particles containing PEG-oleate bilayer ligands for 24 h. First, enzymatic activity of the cells upon exposure to NPs for 24 h was tested though an MTT assay. The result (Figure 4) showed a decrease in metabolic activity for both types of particles tested. The bare particles were the least toxic yet showed some concentration dependent toxicity. Compared to control groups, the bare particles showed minimal toxicity at the lowest concentration tested (i.e., 5 μg/mL) and ∼30% toxicity at the highest concentration (75 μg/mL). The MTT toxicity scaled linearly with R^2 = 0.911 for concentrations between minimum and maximum dose. However, the PEG-oelate NPs had a surprisingly significant effect on the metabolic activity of the cells. The NPs decreased the metabolic activity of the cells to nearly 50% of control levels at all concentrations with only a slight concentration dependence. The results were repeatable for different batches of NPs. Therefore, we pursued further studies to understand the cause and possible mechanism of higher toxicity of the PEG-oleate bilayer NPs.

To confirm the result obtained from the MTT assay, we ran live/dead cell calcein and propidium iodide viability assays. Calcein AM can permeate cell membranes. Though calcein AM itself is not a fluorescent molecule, the calcein generated by esterase in a viable cell emits strong green fluorescence. Therefore, calcein stains only viable cells. On the other hand, propidium iodide (PI), a nucleus-staining dye, cannot pass through a viable cell membrane, thus PI stains only dead cells. It reaches the nucleus by passing through disordered areas of dead cell membrane and intercalates with the DNA double helix of the cell to emit red fluorescence. As shown in Figure 5, the cell counts via calcein staining were significantly reduced following 24 h incubation with the two types of NPs. In agreement with the MTT assay cell viability result, we found that the PEG-oleate bilayer NPs resulted in less viable cells at the 75 μg/mL NP concentration (Figure 5e). To analyze and quantify the result, we used image processing software ImageJ to quantify the cell viability. The analysis showed that PEG-oleate bilayer NPs decreased the cell viability by 50% compared to the control. The bare surface NPs reduced the cell count as well, less significantly, to 67% of control. The PI control cells were released from the surface of the plate upon death, and hence only calcein counts were taken into account. An image of the PI control is shown in Figure S5. From this we conclude that the PEG-oleate bilayer NPs induced significant toxic response to the cells, even at low concentration.

To verify these previously unreported findings of toxicity from bilayer PEGylated NPs, we examined covalently bound PEG-NPs at the same condition for 24 h in a separate experiment. The result is presented in Figure S6. It was found that the HAEC control covered 28.6% of the imaged area, HAECs incubated with covalently bound PEG-NPs covered 32.2%, and PEG-oleate bilayer NPs covered 11.0%. This result

dx.doi.org/10.1021/la501595f | Langmuir 2014, 30, 8167−8176

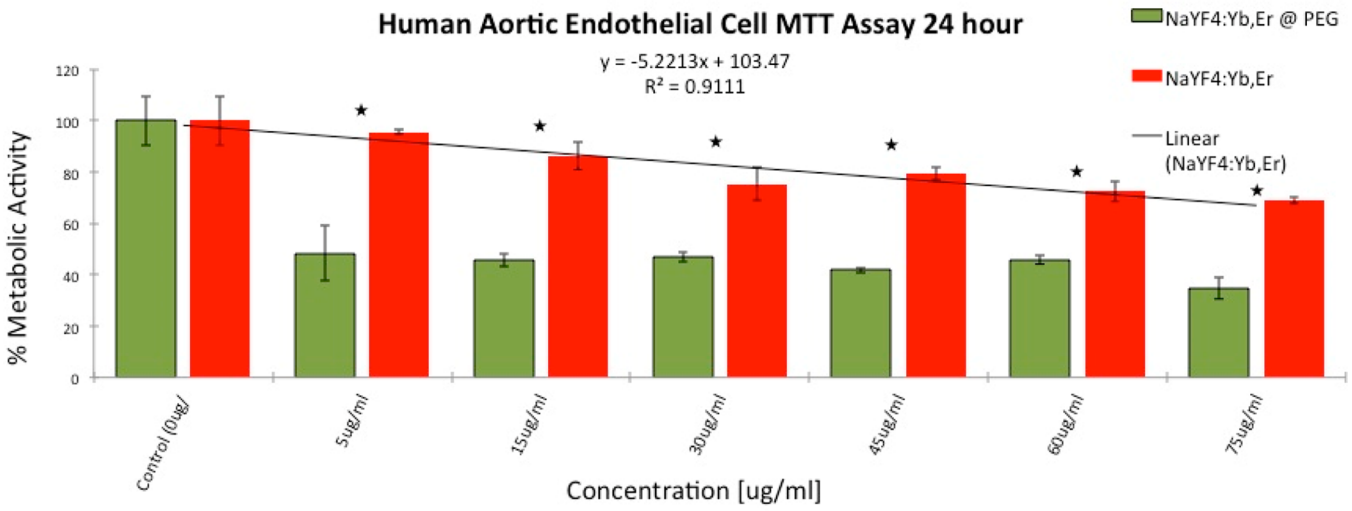

Figure 4. MTT assay comparing metabolic activity of HAEC's incubated with PEG-oleate capped and with bare $NaYF_4$:Yb,Er for 24 h. Experiments were run in triplicate; error bars are ± 1 SD. Linear best fit line $R^2 = 0.911$. Stars indicate a significant difference via *p*-tests between toxicity levels at each concentration with *p*-values < 0.01.

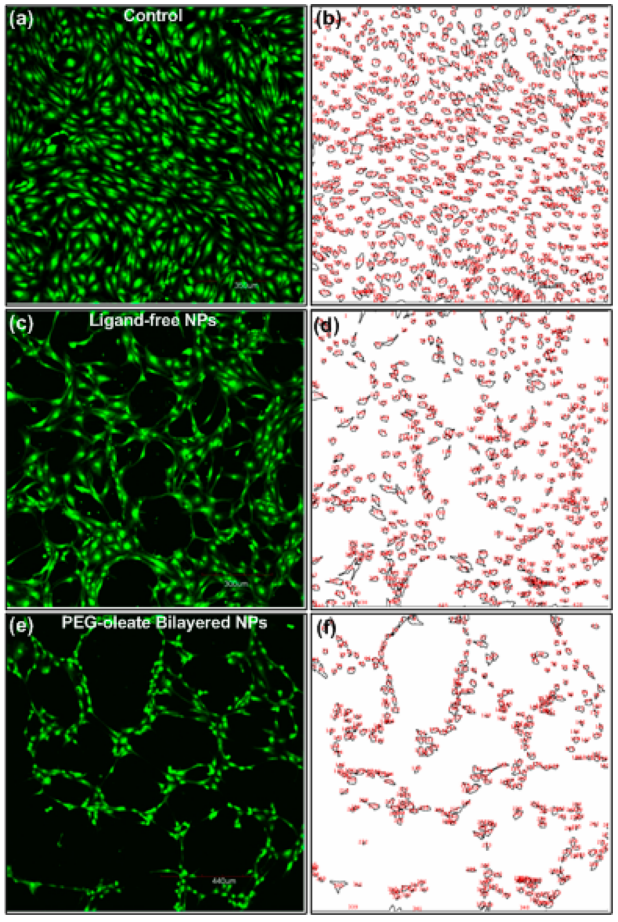

Figure 5. Fluorescent images of cells from calcein assays (a,c,e), and quantification analysis of the confocal fluorescent images using ImageJ analysis (b,d,f). All cells were incubated with 75 μg/mL NPs for 24 h. Surface area and cell count normalized by calcein control. Analysis show that ligand-free $NaYF_4$:Yb,Er NPs (c,d) resulted in 67% viable cells, while PEG-oleate bilayered NPs (e,f) had 50% viable cells compared to control.

conclusively showed that the PEG-oleate NPs induced the observed toxicity. The impact of ligands on toxicity is not altogether unknown—an earlier study reported a ligand-based toxicity of iron oxide NPs.[3] In that case, the iron oxide was nontoxic, but different types of surface ligands gave rise to toxicity in HepG2 cells. The effect was attributed to the surface ligands rather than the nanoparticles themselves.

We examined the role of the ligands in our case. To determine the amount of ligands present on the NPs, TGA was performed (Figure S7). As seen in Figure S7, about 9% of the nanoparticle mass was attributable to the additional PEG-oleate layer. We calculated the equivalent PEG present in the 9% PEG-oleate ligand then used equivalent amounts (3.97 μg/mL or 4.61 μM) of both PEG and PEG-oleate to assess their cytotoxicity independently of the nanoparticles. The concentration used in the control experiments (i.e., 4.61 μM) is below the critical micelle concentration (CMC) reported for similar PEG-fatty acids (i.e., 9.91 μM) in the literature.[39,40] It is also worth noting that only about 2% weight loss was observed for the bare NPs in a TGA analysis; the weight loss is attributed to the residual ligands on the bare NPs. The ligand content on all three NPs is in good agreement with the literature data.[41] As shown by the calcein assay in Figure 6, no signs of toxicity were observed after 24 h incubation with either type of ligand.

Generally, PEG is known to be nontoxic, hence the result was expected. However, the relatively benign behavior of the PEG-oleate ligand was most likely due to formation of micelles, thus secluding the hydrophobic oleate molecules in the micelle and exposing PEG chains to the culture media. Therefore, cells were only exposed to PEG, which resulted in no toxicity. Based on this observation, we ruled out the possibility that our observed NP toxicity is due to excess PEG-oleate ligands present in the NP dispersion. We hypothesized that the toxicity might arise from the partial or complete dissociation of the oleate-capping on the NPs themselves.

We tested our hypothesis first by analyzing the cell growth medium. The PEG-oleate NPs exhibited a unique behavior upon incubation with a confluent monolayer of HAEC's. After a 24 h incubation with the PEG-oleate bilayer $NaYF_4$:Yb,Er, a white precipitate was observed to settle on the bottom of the culture dish. This precipitation only occurred with the PEG-

dx.doi.org/10.1021/la501595f | *Langmuir* 2014, 30, 8167−8176

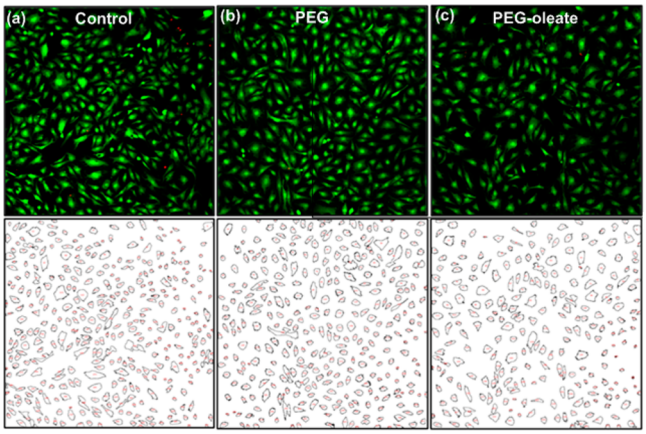

Figure 6. Fluorescent images of cells obtained from calcein assays (top panel), and quantification analysis of the confocal fluorescent images using ImageJ analysis (bottom panel) of (a) control cells, and cells treated with (b) PEG (M_w = 2000), and (c) PEG-oleate (M_w = 860). All showed similar cell viability and cell counts.

oleate $NaYF_4$:Yb,Er NPs—not with the other two types of NPs. Photographs of active cultures and the collected supernatant are shown in Figure 7. This observation suggested that

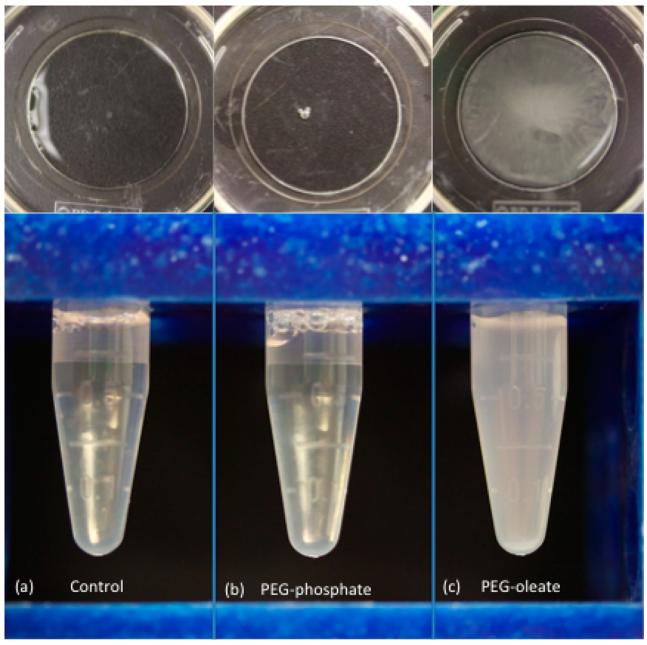

Figure 7. Observation of white precipitate/cloudy solution after a 24 h incubation with the PEG-oleate bilayered $NaYF_4$:Yb,Er NPs (c: far right panel) while the covalent PEG-NPs (b: middle panel) and control (a: far left panel) resulted in clear supernatant. (Top panels) Mattek cell culture dishes after a 24 h incubation of the respective NPs with cells.

bilayered PEG-oleates may dissociate during their interaction with cells. To investigate this possibility, an aliquot of the conditioned medium from the PEG-oleate bilayer $NaYF_4$:Yb,Er incubation was taken for analysis. It was first mixed well with an equal volume of hexane, followed by the separation of organic layers. It was expected that the oleate molecules would move to the organic layer due to their higher affinity for hexane. The organic layer was then dried in a vacuum oven and the remaining waxy liquid was analyzed with FTIR. As seen in Figure S3c, the waxy layer showed all the peaks that matched PEG and oleic acid. Hence, we identified the waxy material as the PEG-oleate ligands used for NP phase transfer. This experiment provided confirmation of our hypothesis that ligand dissociation could result in a particle surface that was capped with oleates only.

To investigate the mechanism of ligand dissociation, we suspended the PEG-oleate $NaYF_4$:Yb,Er NPs in (i) fresh medium and (ii) medium conditioned by growing cells. In fresh medium (i.e., never used in cell culture), no precipitation was observed at the 75 μg/mL concentration after 24 h. However, when NPs were suspended for 24 h in conditioned medium (i.e., medium gathered from a 95% confluent HAEC culture flask grown for 24 h), we observed the formation of white precipitate. We hypothesized that changes in pH and ionic concentration of the media caused by the cell culture may have destabilized the PEG-oleate nanoparticles. However, pH and ionic conductivity measurements taken over a 24 h incubation showed minimal changes, all of which were within a range to preserve particle stability. To further understand the observations, the collected conditioned medium was denatured at 100 °C for 4 h before running the experiment again. Upon completion, we observed that in the unmodified conditioned medium, the sample became cloudy and a white precipitate had begun to settle out—on the other hand, the denatured conditioned medium had only the slightest hint of precipitate formation. From this result, we concluded that the nanoparticles that transferred from one phase to another via a bilayer formation may not be stable and useful in biological applications. We propose that the PEG-oleate $NaYF_4$:Yb,Er NPs undergo a deintercalation process that is initiated by an extra-cellular protein or enzyme produced by the cell. This reaction is largely eliminated by the denaturing of the extracellular proteins.

Confocal microscopy was employed to examine the cellular localization of the NPs. Due to their unique up-converting optical properties, we were able to excite the NPs within the cells using a low energy near-infrared (NIR) laser (980 nm). NIR excitation also minimizes cellular autofluorescence. As shown in Figure 8, fluorescence from the NPs was distinctly observed within the cells. The NPs were localized mainly in the cytoplasmic and perinuclear regions.

The internalization of the NPs provided insight into the interaction of the PEG-oleate bilayered NP with the cells. Based on NP internalization, observed through confocal microscopy, we propose the mechanism depicted in Figure 9. We suggest that the oleate bound to the NPs is most likely the cause of cytotoxicity. Yin et al.[42] investigated the impact of oleic acid on cytotoxicity using nickel ferrite particles in neuro-2A cells. Their study revealed that cell membranes have the capability to accumulate some oleic acid molecules within the lipid bilayer due to their hydrophobic nature. They also noted that at high concentrations, cellular viability dropped drastically, to as low as 10% for the highest concentration they used. With regard to the PEG-oleate bilayer NPs, we propose that as ligand dissociation takes place, initiated by cell-secreted enzymes, the separated PEG-oleate layer formed micelles and remained suspended in the cell culture medium as characterized by FTIR. However, the resultant NPs capped with oleates passed through the lipid bilayer and resulted in the observed drop in cellular viability. Due to the oleate induced toxicity, low cell viability was observed even at very low NP concentrations (e.g., 5–10 μg/mL). We believe that the lowest concentration of the

dx.doi.org/10.1021/la501595f | Langmuir 2014, 30, 8167–8176

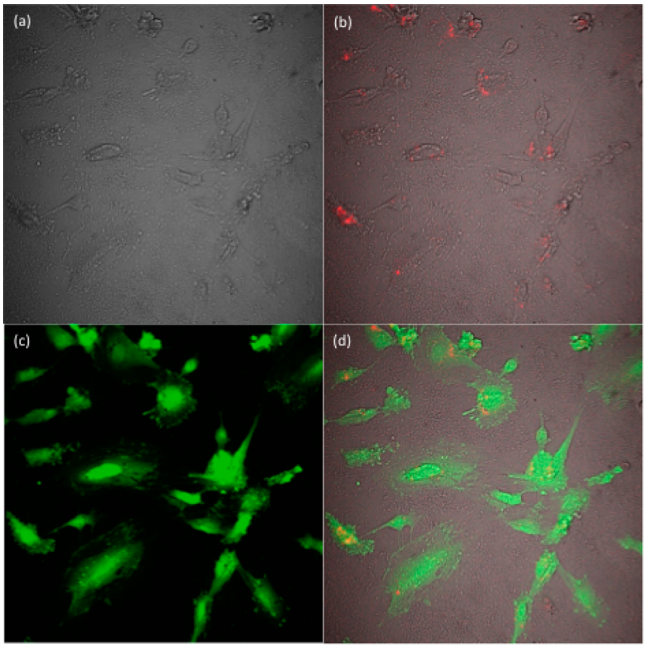

Figure 8. Confocal microscope images of the HAEC cells (a) bright field image of the cells, (b) PEG-oleate bilayered NPs internalized by the cells excited with a 980 nm excitation laser (NPs are false colored as red), (c) fluorescent signal from calcein, and (d) overlay of a–c.

oleate-capped NPs had sufficient oleates to saturate the metabolic response of the mitochondria, reflected in the lack of a dose dependent response. Although oleate-induced cytotoxicity has been reported in previous studies, ligand dissociation from a phase-transferred NP, leading to cytotoxicity, is a unique observation.

Finally, we confirmed the result with another subset of lanthanide NPs, viz., $NaGdF_4$:Yb,Er (Figure S8, avg. size ~13 nm) which have been widely studied for MRI and optical imaging applications. We synthesized the NPs and functionalized the surface in exactly the same way as the $NaYF_4$:Yb,Er. An MTT assay shows (Figure 10) the same trend that was observed for $NaYF_4$:Yb,Er for both the bare and PEG-oleate bilayer NPs. We conclude that there is a general potential for ligand dissociation in bilayered PEG-oleate ligands which can lead to toxicity by exposing cells to oleates.

■ CONCLUSION

It has been found that it is crucial to consider not only the intrinsic potential toxicity of nanomaterials that are applied to living systems, but also to consider the type of ligands that are used to functionalize or passivate particles and how they are attached. The particular material in this case was an up-converting phosphor NP that by itself appeared to pose a limited dose-dependent potential for toxicity. However, capping the particles with oleates introduced a significant risk of toxicity

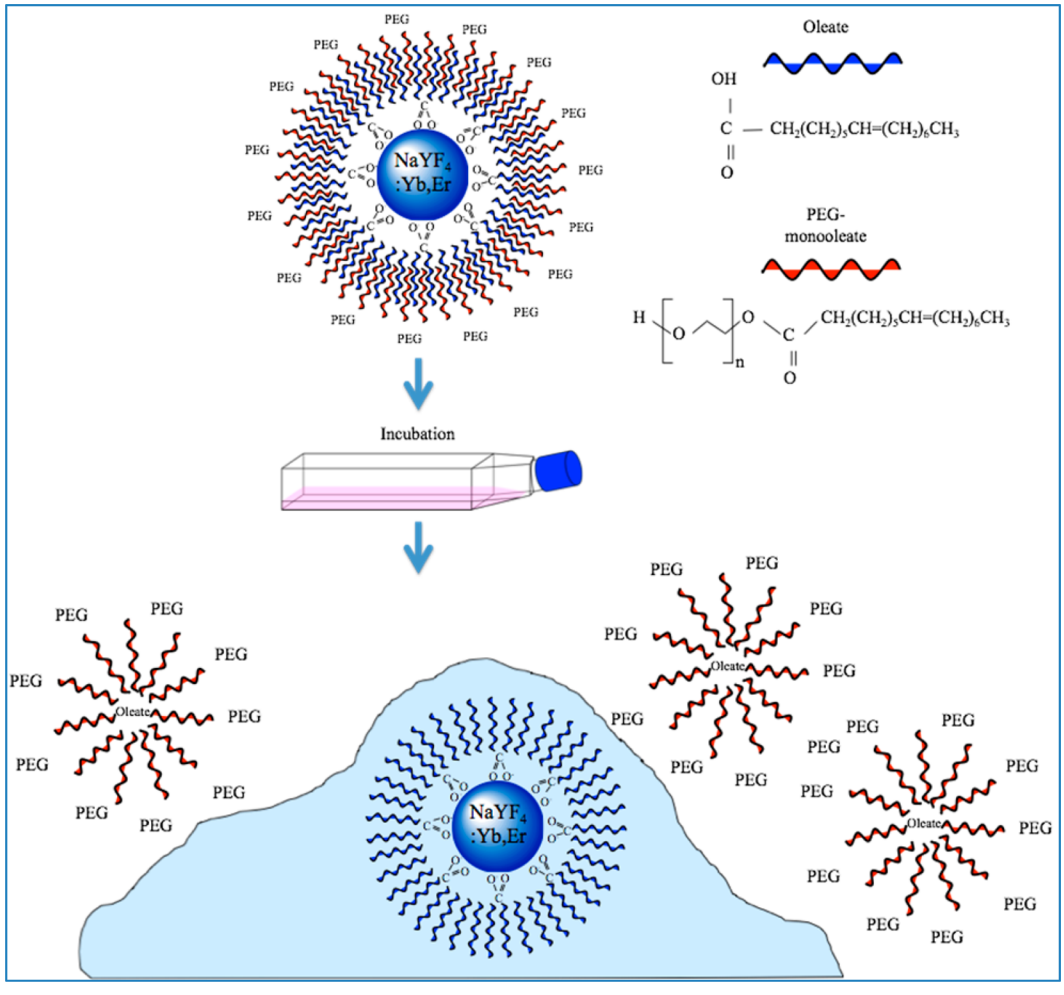

Figure 9. Proposed schematic of dissociation mechanism of PEG-oleate bilayered NPs and internalization in cells.

dx.doi.org/10.1021/la501595f | *Langmuir* 2014, 30, 8167–8176

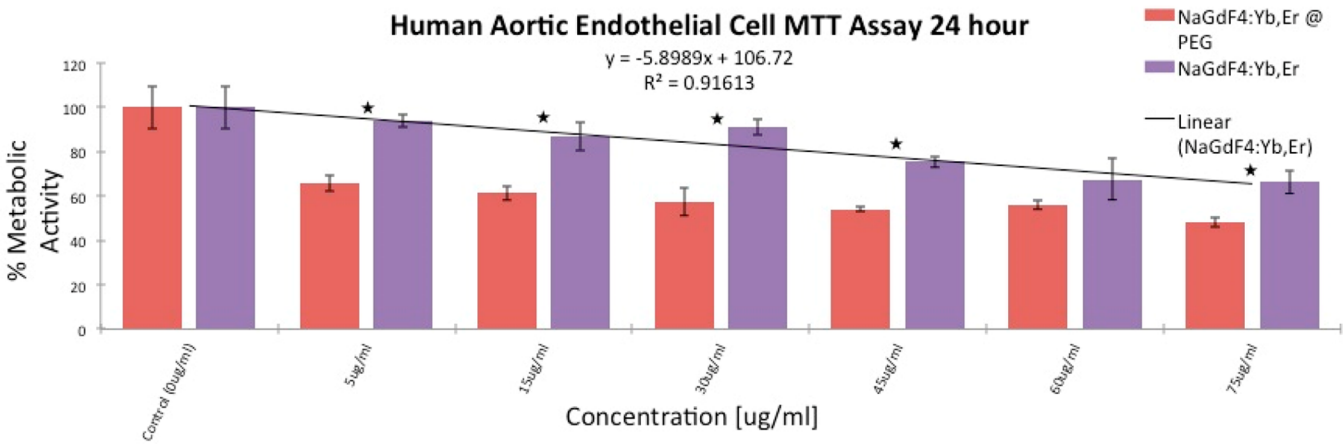

Figure 10. MTT assay comparing metabolic activity of HAEC's incubated with PEG-oleate capped and with bare $NaGdF_4$:Yb,Er for 24 h. Experiments were run in triplicate, error bars are ± 1 SD. Linear best fit line $R^2 = 0.916$. Stars indicate a significant difference via *p*-tests between toxicity levels at each concentration with *p*-values < 0.01.

to cells. Because this class of NPs is mostly synthesized in a high temperature reaction with a hydrophobically coordinated ligand such as oleic acid, they can be potentially toxic if weakly coordinated surface groups are used to render them biocompatible. This study has shown that intercalated ligands can result in oleate-capped NPs upon interaction with cells, rendering them cytotoxic. An improved understanding of the interaction of this common capping agent with cells can be used to design and construct improved nanoparticles for a range of bioapplications where particle stability and biocompatibility are extremely important.

■ ASSOCIATED CONTENT

Ⓢ Supporting Information

Figure S1−S8. Zeta potential, FTIR, XRD, TGA, and TEM micrograph of the nanoparticle and cell image. This material is available free of charge via the Internet at http://pubs.acs.org

■ AUTHOR INFORMATION

Corresponding Author

*E-mail: imkennedy@ucdavis.edu.

Author Contributions

†Authors with equal contributions

Notes

The authors declare no competing financial interest.

■ ACKNOWLEDGMENTS

The project was supported by the W. M. Keck Foundation with a research grant in science and engineering. This material is also based upon work supported by the National Science Foundation Graduate Research Fellowship under Grant No. 1148897. We acknowledge the support of Award Number P42ES004699 from the National Institute of Environmental Health Sciences. The content is solely the responsibility of the authors and does not necessarily represent the official views of the National Science Foundation or the National Institute of Environmental Health Sciences.

■ REFERENCES

(1) Dong, A.; Ye, X.; Chen, J.; Kang, Y.; Gordon, T.; Kikkawa, J. M.; Murray, C. B. A Generalized Ligand-Exchange Strategy Enabling Sequential Surface Functionalization of Colloidal Nanocrystals. *J. Am. Chem. Soc.* **2010**, *133* (4), 998−1006.

(2) Nel, A. E.; Madler, L.; Velegol, D.; Xia, T.; Hoek, E. M. V.; Somasundaran, P.; Klaessig, F.; Castranova, V.; Thompson, M. Understanding Biophysicochemical Interactions at the Nano−Bio Interface. *Nat. Mater.* **2009**, *8* (7), 543−557.

(3) Tan, S. J.; Jana, N. R.; Gao, S.; Patra, P. K.; Ying, J. Y. Surface−Ligand-Dependent Cellular Interaction, Subcellular Localization, and Cytotoxicity of Polymer-Coated Quantum Dots. *Chem. Mater.* **2010**, *22* (7), 2239−2247.

(4) Kim, S. T.; Saha, K.; Kim, C.; Rotello, V. M. The Role of Surface Functionality in Determining Nanoparticle Cytotoxicity. *Acc. Chem. Res.* **2013**, *46* (3), 681−691.

(5) Prakash, A.; Zhu, H.; Jones, C. J.; Benoit, D. N.; Ellsworth, A. Z.; Bryant, E. L.; Colvin, V. L. Bilayers as Phase Transfer Agents for Nanocrystals Prepared in Nonpolar Solvents. *ACS Nano* **2009**, *3* (8), 2139−2146.

(6) Nam, J.; Won, N.; Bang, J.; Jin, H.; Park, J.; Jung, S.; Jung, S.; Park, Y.; Kim, S. Surface Engineering of Inorganic Nanoparticles for Imaging and Therapy. *Adv. Drug Delivery Rev.* **2013**, *65* (5), 622−648.

(7) Wu, H.; Zhu, H.; Zhuang, J.; Yang, S.; Liu, C.; Cao, Y. C. Water-Soluble Nanocrystals through Dual-Interaction Ligands. *Angew. Chem., Int. Ed.* **2008**, *47* (20), 3730−3734.

(8) Shan, J. N.; Chen, J. B.; Meng, J.; Collins, J.; Soboyejo, W.; Friedberg, J. S.; Ju, Y. G. Biofunctionalization, Cytotoxicity, and Cell Uptake of Lanthanide Doped Hydrophobically Ligated $NaYF_4$ Upconversion Nanophosphors. *J. Appl. Phys.* **2008**, *104* (9).

(9) Xiong, L. Q.; Yang, T. S.; Yang, Y.; Xu, C. J.; Li, F. Y. Long-Term in Vivo Biodistribution Imaging and Toxicity of Polyacrylic Acid-Coated Upconversion Nanophosphors. *Biomaterials* **2010**, *31* (27), 7078−7085.

(10) Zhou, J. C.; Yang, Z. L.; Dong, W.; Tang, R. J.; Sun, L. D.; Yan, C. H. Bioimaging and Toxicity Assessments of near-Infrared Upconversion Luminescent $NaYF_4$:Yb,Tm Nanocrystals. *Biomaterials* **2011**, *32* (34), 9059−9067.

(11) Abdul Jalil, R.; Zhang, Y. Biocompatibility of Silica Coated NaYF4 Upconversion Fluorescent Nanocrystals. *Biomaterials* **2008**, *29* (30), 4122−4128.

(12) Sperling, R. A.; Parak, W. J. Surface Modification, Functionalization and Bioconjugation of Colloidal Inorganic Nanoparticles. *Philos. Trans. R. Soc. A* **2010**, *368* (1915), 1333−1383.

(13) Cheng, L.-C.; Jiang, X.; Wang, J.; Chen, C.; Liu, R.-S. Nano−Bio Effects: Interaction of Nanomaterials with Cells. *Nanoscale* **2013**, *5* (9), 3547−3569.

(14) Fricker, S. P. The Therapeutic Application of Lanthanides. *Chem. Soc. Rev.* **2006**, *35* (6), 524−533.

(15) Gnach, A.; Bednarkiewicz, A. Lanthanide-Doped Up-Converting Nanoparticles: Merits and Challenges. *Nano Today* **2012**, *7* (6), 532−563.

(16) Lee, S. S.; Zhu, H.; Contreras, E. Q.; Prakash, A.; Puppala, H. L.; Colvin, V. L. High Temperature Decomposition of Cerium Precursors to Form Ceria Nanocrystal Libraries for Biological Applications. *Chem. Mater.* **2011**, *24* (3), 424−432.
(17) Das, G. K.; Johnson, N. J. J.; Cramen, J.; Blasiak, B.; Latta, P.; Tomanek, B.; van Veggel, F. C. J. M. $NaDyF_4$ Nanoparticles as T2 Contrast Agents for Ultrahigh Field Magnetic Resonance Imaging. *J. Phys. Chem. Lett.* **2012**, *3* (4), 524−529.
(18) Pichaandi, J.; Boyer, J.-C.; Delaney, K. R.; van Veggel, F. C. J. M. Two-Photon Upconversion Laser (Scanning and Wide-Field) Microscopy Using Ln^{3+}-Doped $NaYF_4$ Upconverting Nanocrystals: A Critical Evaluation of their Performance and Potential in Bioimaging. *J. Phys. Chem. C* **2011**, *115* (39), 19054−19064.
(19) Verma, A.; Stellacci, F. Effect of Surface Properties on Nanoparticle−Cell Interactions. *Small* **2010**, *6* (1), 12−21.
(20) Yeh, Y.-C.; Saha, K.; Yan, B.; Miranda, O. R.; Yu, X.; Rotello, V. M. The Role of Ligand Coordination on the Cytotoxicity of Cationic Quantum Dots in HeLa Cells. *Nanoscale* **2013**, *5* (24), 12140−12143.
(21) Wang, F.; Banerjee, D.; Liu, Y.; Chen, X.; Liu, X. Upconversion Nanoparticles in Biological Labeling, Imaging, and Therapy. *Analyst* **2010**, *135* (8), 1839−1854.
(22) Chatterjee, D. K.; Gnanasammandhan, M. K.; Zhang, Y. Small Upconverting Fluorescent Nanoparticles for Biomedical Applications. *Small* **2010**, *6* (24), 2781−2795.
(23) Sun, L.-D.; Wang, Y.-F.; Yan, C.-H. Paradigms and Challenges for Bioapplication of Rare Earth Upconversion Luminescent Nanoparticles: Small Size and Tunable Emission/Excitation Spectra. *Acc. Chem. Res.* **2014**, *47*, 1001−1009.
(24) Ye, X.; Collins, J. E.; Kang, Y.; Chen, J.; Chen, D. T. N.; Yodh, A. G.; Murray, C. B. Morphologically Controlled Synthesis of Colloidal Upconversion Nanophosphors and Their Shape-Directed Self-Assembly. *Proc. Natl. Acad. Sci. U. S. A.* **2010**, *107* (52), 22430−22435.
(25) Lakshmana, S.; Das, G. K.; Li, C.; Stark, D.; Cena, J.; Cherry, S.; Kennedy, I. M. $NaGdF_4$:Eu^{3+} Nanoparticles for Enhanced X-ray Excited Optical Imaging. *Chem. Mater.* **2014**, *26* (5), 1881−1888.
(26) Chen, G.; Yang, C.; Prasad, P. N. Nanophotonics and Nanochemistry: Controlling the Excitation Dynamics for Frequency Up- and Down-Conversion in Lanthanide-Doped Nanoparticles. *Acc. Chem. Res.* **2013**, *46* (7), 1474−1486.
(27) Jańczewski, D.; Zhang, Y.; Das, G. K.; Yi, D. K.; Padmanabhan, P.; Bhakoo, K. K.; Tan, T. T. Y.; Selvan, S. T. Bimodal Magnetic−Fluorescent Probes for Bioimaging. *Microsc. Res. Tech.* **2011**, *74* (7), 563−576.
(28) Xie, X.; Gao, N.; Deng, R.; Sun, Q.; Xu, Q.-H.; Liu, X. Mechanistic Investigation of Photon Upconversion in Nd^{3+}-Sensitized Core−Shell Nanoparticles. *J. Am. Chem. Soc.* **2013**, *135* (34), 12608−12611.
(29) Gai, S.; Li, C.; Yang, P.; Lin, J. Recent Progress in Rare Earth Micro/Nanocrystals: Soft Chemical Synthesis, Luminescent Properties, and Biomedical Applications. *Chem. Rev.* **2014**, *114*, 2343−2389.
(30) Zhang, Y.; Vijayaragavan, V.; Das, G. K.; Bhakoo, K. K.; Tan, T. T. Y. Single-Phase $NaDyF_4$:Tb^{3+} Nanocrystals as Multifunctional Contrast Agents in High-Field Magnetic Resonance and Optical Imaging. *Eur. J. Inorg. Chem.* **2012**, *2012* (12), 2044−2048.
(31) Heng, B.; Das, G.; Zhao, X.; Ma, L.-L.; Tan, T.-Y.; Ng, K.; Loo, J.-C.; Ma, L.-L. Comparative Cytotoxicity Evaluation of Lanthanide Nanomaterials on Mouse and Human Cell Lines with Metabolic and DNA-Quantification Assays. *Biointerphases* **2010**, *5* (3), FA88−FA97.
(32) Das, G. K.; Chan, P. P. Y.; Teo, A.; Loo, J. S. C.; Anderson, J. M.; Tan, T. T. Y. In Vitro Cytotoxicity Evaluation of Biomedical Nanoparticles and Their Extracts. *J. Biomed. Mater. Res. A* **2010**, *93A* (1), 337−346.
(33) Cheng, L.; Yang, K.; Zhang, S.; Shao, M.; Lee, S.; Liu, Z. Highly-Sensitive Multiplexed in Vivo Imaging Using Pegylated Upconversion Nanoparticles. *Nano Res.* **2010**, *3* (10), 722−732.
(34) Budijono, S. J.; Shan, J.; Yao, N.; Miura, Y.; Hoye, T.; Austin, R. H.; Ju, Y.; Prud'homme, R. K. Synthesis of Stable Block-Copolymer-Protected $NaYF_4$:Yb^{3+}, Er^{3+} Up-Converting Phosphor Nanoparticles. *Chem. Mater.* **2009**, *22* (2), 311−318.
(35) Tan, M. C.; Al-Baroudi, L.; Riman, R. E. Surfactant Effects on Efficiency Enhancement of Infrared-to-Visible Upconversion Emissions of $NaYF_4$:Yb−Er. *ACS Appl. Mater. Interfaces* **2011**, *3* (10), 3910−3915.
(36) Li, Z.; Zhang, Y. An Efficient and User-Friendly Method for the Synthesis of Hexagonal-Phase $NaYF_4$:Yb,Er/Tm Nanocrystals with Controllable Shape and Upconversion Fluorescence. *Nanotechnology* **2008**, *19* (34), 345606.
(37) Bogdan, N.; Vetrone, F.; Ozin, G. A.; Capobianco, J. A. Synthesis of Ligand-Free Colloidally Stable Water Dispersible Brightly Luminescent Lanthanide-Doped Upconverting Nanoparticles. *Nano Lett.* **2011**, *11* (2), 835−840.
(38) Boyer, J.-C.; Manseau, M.-P.; Murray, J. I.; van Veggel, F. C. J. M. Surface Modification of Upconverting $NaYF_4$ Nanoparticles with PEG−Phosphate Ligands for NIR (800 nm) Biolabeling within the Biological Window. *Langmuir* **2009**, *26* (2), 1157−1164.
(39) Yang, J.; Lee, T.-I.; Lee, J.; Lim, E.-K.; Hyung, W.; Lee, C.-H.; Song, Y. J.; Suh, J.-S.; Yoon, H.-G.; Huh, Y.-M.; Haam, S. Synthesis of Ultrasensitive Magnetic Resonance Contrast Agents for Cancer Imaging Using PEG-Fatty Acid. *Chem. Mater.* **2007**, *19* (16), 3870−3876.
(40) van Gruijthuijsen, K.; Rufier, C.; Phou, T.; Obiols-Rabasa, M.; Stradner, A. Light and Neutron Scattering Study of PEG-oleate and Its Use in Emulsion Polymerization. *Langmuir* **2012**, *28* (28), 10381−10388.
(41) Wang, M.; Chen, Z.; Zheng, W.; Zhu, H.; Lu, S.; Ma, E.; Tu, D.; Zhou, S.; Huang, M.; Chen, X. Lanthanide-Doped Upconversion Nanoparticles Electrostatically Coupled with Photosensitizers for Near-Infrared-Triggered Photodynamic Therapy. *Nanoscale* **2014**, *6*, 8274−8282.
(42) Yin, H.; Too, H. P.; Chow, G. M. The Effects of Particle Size and Surface Coating on the Cytotoxicity of Nickel Ferrite. *Biomaterials* **2005**, *26* (29), 5818−5826.